Journal of Materials Chemistry A

Accepted Manuscript

ROYAL SOCIETY OF CHEMISTRY

www.rsc.org/materialsA

Manuscript ID: TA-ART-03-2015-001760.R1

Al Conductive Haloaluminate-free Non-aqueous Room-Temperature Electrolytes

Toshihiko Mandai[†,*] *and Patrik Johansson*[†,‡]

[†]Department of Applied Physics, Chalmers University of Technology, SE-412 96 Göteborg, Sweden

[‡]Current position: Visiting professor at LRCS/CNRS UMR7314, Université de Picardie Jules Verne, 33 rue Saint Leu, 80039 Amiens, France

CORRESPONDING AUTHOR FOOTNOTES

Telephone: +46-31-772-3310, E-mail: mandi@chalmers.se

Abstract

Al batteries are yet rather unexplored as a promising technology to respond the growing electrochemical energy storage demands. Despite outstanding electrochemical activity of haloaluminate-based electrolytes, no prospect of practical re-chargeable Al batteries has yet been materialized, partly due to these electrolytes' extremely sensitive nature. Hence alternative aluminum conducting electrolytes with sufficient stability are strongly urged for. Here a series of room-temperature ternary electrolytes consisting of aluminum trifluoromethanesulfonate ($Al[TfO]_3$), *N*-methylacetamide (NMA), and urea are presented, which provide excellent ionic conductivities by selecting appropriate ratios. Compared to conventional organic electrolytes, unprecedented solvation ability for Al-salts and remarkable ion transport properties were observed. For the optimized composition; $Al[TfO]_3$/NMA/urea = 0.05/0.76/0.19, physicochemical properties and vibrational spectroscopy data implies a decoupling of the Al conduction mechanism from viscosity limitations and furthermore that the dissociation state of the $Al[TfO]_3$ salt drastically changes. These phenomena are likely due to the unique coordination environment of the Al^{3+} ions and the multiple functions of urea in these ternary mixtures. The electrochemical properties of the optimized ternary electrolyte were studied with respect to the electrochemical stability window and using cyclic voltammetry.

Key Word: Al electrolyte, ternary mixture, physicochemical properties, spectroscopy

Introduction

The dramatic progress in large-scale mobile electric applications, such as the electromobility revolution, requires novel highly efficient electrochemical energy storage systems with enhanced safety to fulfill their full potential. Post lithium-ion batteries, especially those incorporating multivalent metals as anodes, are promising technologies to respond these demands due to their high capacities.[1] While the reduction potentials of applicable multivalent metals, such as magnesium, zinc, and aluminium, all are higher than that of lithium metal (−3.04 V *vs*. SHE), their large volumetric and/or specific (gravimetric) capacities still offer possibilities for enhanced electrochemical energy storage systems compared to present Li-ion batteries. Ion-conductive materials for shuttling Mg^{2+}, Zn^{2+}, or Al^{3+} species are urged for, as these batteries' performance is strongly limited by the ion-conductive media available. Many attempts have therefore been made to accomplish high performance multivalent ion-conductive materials, including liquid, solid, and polymer electrolytes.[2–10] Only a few systems, however, have achieved any favorable ionic conductivities, much due to the very strong ion–ion interactions between the multivalent metal cations and their counter anions, which must be surpassed by ion–solvent interactions. This basic feature restricts the possible salt and solvent combinations to solvents with high polarity and/or good solvating power, and highly dissociative salts based on charge-delocalized weak Lewis basic anions, regardless of the metal-ion battery concept chosen.[11–13]

Another path is using mutually miscible compounds to lower the resulting melting point, compared to the individual components, by an entropic effect, for appropriate ratios resulting in a

homogeneous liquid at ambient temperature. The most extensively studied metal-containing room temperature melt/electrolyte systems so far are those composed of $AlCl_3$ and various solid organic compounds.[14–18] Other examples are $ZnCl_2$ and $NiCl_2$, which both form room temperature melts/electrolytes by mixing with dialkylsolfone.[19,20] In addition to systems involving metal halide salts, most often Cl based, binary systems composed of inorganic nitrates and acetamides also have been shown to produce low-melting eutectics.[21] Indeed, many solid organic compounds with an acylamino group present, such as urea, acetamide, and their derivatives, lower the melting point of mixtures and consequently lead to form metal-containing room temperature electrolytes.[18,21–26] Acylamino-based compounds interact with both cations and anions, why mixtures of the LiTFSA/LiTFSI salt, based on the weakly Lewis basic bis(trifluoromethanesulfonyl)amide/imide TFSA/TFSI anion, with urea, acetamide, or *N*-methylacetamide (NMA) result in room temperature molten electrolytes with high ionic conductivities.[22–24] The excellent solvation ability facilitates to even dissociate salts of divalent metal ions and/or relatively strong Lewis basic anions such as ClO_4^- or $[TfO]^-$ enabling to form Mg-conductive room temperature electrolytes based on magnesium perchlorate, $Mg(ClO_4)_2$, or magnesium trifluoromethanesulfonate, $Mg[TfO]_2$, mixed with acetamide and urea.[26]

Owing to these remarkable features, metal-containing room-temperature melts/electrolytes are promising as ion-conductive media for various applications *e.g.* as electrolytes for Li, Mg, and Al batteries.[10,18,22–24,26–29] As for Al batteries, almost all non-aqueous electrolytes studied incorporate $AlCl_3$. Due to the highly reactive and corrosive nature of $AlCl_3$, however, development of $AlCl_3$-free

electrolytes is crucial to realize practical Al batteries. In this paper, we report on ternary electrolyte systems comprising a halide-free Al salt ($Al[TfO]_3$), NMA, and urea. The replacement of $AlCl_3$ by $Al[TfO]_3$, inert towards air and moisture, can address the safety issues of $AlCl_3$. Owing to successful application of ternary melt electrolytes for Mg batteries[26] and the somewhat analogous electrochemistry of Mg and Al batteries,[1] the Al-based analogues are conceptually possible to apply in Al batteries as electrolytes. As ternary mixtures of $Al[TfO]_3$, acetamide, and urea remain in solid state even at 50 ºC, we replace acetamide by NMA, to accomplish room temperature electrolytes. Basic physicochemical properties of ternary electrolytes are reported including density, viscosity, and ionic conductivity, and are compared to those of various organic solvent based electrolytes. Furthermore, both IR and Raman spectroscopies were used to in detail reveal the state of the charge carriers for various ternary electrolyte compositions.

Experimental

Materials

$Al[TfO]_3$ (99.9% trace metals basis), diethyl carbonate (DEC; anhydrous, 99%), tetrahydrofuran (THF; anhydrous, 99.9%), dimethoxyethane (G1; anhydrous, 99.5%), triglyme (G3; 99%), tetraglyme (G4; 99%), acetonitrile (ACN; anhydrous, 99.8%), propylene carbonate (PC; anhydrous, 99.7%), *N*-methylacetamide (NMA; 99%), urea (99%), aluminum chloride ($AlCl_3$; anhydrous, 99.99% trace metals basis), and 1-ethyl-3-methylimidazolium chloride (EMImCl; 98%) were all purchased from Sigma-Aldrich. $Al[TfO]_3$, NMA, urea, and EMImCl were dried under high

vacuum at 80 ºC for 48 h, then stored in an Ar-filled glovebox (< 2 ppm O_2, < 0.5 ppm H_2O) prior to use. G3 and G4 were dried over molecular sieves 4A for several days. The other anhydrous materials were used as received. $Al[TfO]_3$/NMA/urea ternary electrolytes, with the mole fraction of NMA in the range x_{NMA} = 0.475–0.832, and conventional organic electrolytes were prepared by mixing stoichiometric amounts of $Al[TfO]_3$ and solvents inside the glovebox. Although $Al[TfO]_3$ is miscible with certain NMA/urea mixtures to form liquids at ambient temperatures up to 0.10 mole fraction, the resulting liquids are extremely viscous and hence possess poor ionic conductivity. In this study, the mole fraction of $Al[TfO]_3$ in the electrolytes was therefore fixed to 0.050 (molar ratio $Al[TfO]_3$:solvents = 1:19). For the ternary electrolytes, NMA was melted at 40 ºC and the appropriate amounts of $Al[TfO]_3$ and urea were added, and subsequently stirred together overnight to achieve homogeneous clear liquids. Hereafter, all ternary electorlytes are abbreviated as **M**(x_{NMA}) based on the mole fraction of NMA. The EMImCl/$AlCl_3$ acidic melt was prepared as a reference electrolyte by slowly adding $AlCl_3$ to EMImCl to reach a final 1.5:1 molar ratio and then stirred for 12 hours at ambient temperature.

Measurements

The ternary and organic electrolytes were characterized with respect to density, viscosity, and ionic conductivity in the temperature range 20–90 ºC. The densities (ρ) and viscosities (η) were measured using a DMA 4500M and Lovis 2000ME, respectively (Anton Paar), and the former was used to calculate the salt concentration (c) for each system. The ionic conductivity (σ) was determined by dielectric spectroscopy using a Novocontrol broadband dielectric spectrometer in the

frequency range of 10^{-1}–10^{7} Hz. The liquid samples were placed between stainless steel electrodes, fixing as 3.5 mm in diameter and 1.05 mm in thickness with a Teflon spacer. The conductivity cell was assembled in the glovebox and transferred into a cryo-furnace. To maintain a dry-inert atmosphere, the measurements were carried out under a steady flow of nitrogen gas. The DC conductivity was defined as the low-frequency plateau in the frequency-dependent (AC) conductivity plot. For each measurement, the samples were thermally equilibrated at the desired temperature for 30 min. Using the conductivities obtained, the molar conductivity (Λ) was calculated for each system as σ/c. The glass transition temperature (T_g) for the ternary electrolytes was determined by differential scanning calorimetry using DSC Q1000 (TA instruments). The samples were hermetically sealed in aluminum pans inside the Ar-filled glovebox. All sample pans were first annealed at 50 ºC for 30 min, whereafter a scan rate of 10 ºC min^{-1} was used and a temperature range of −150 – +100 ºC was measured. The onset in heat capacity change was taken as the T_g. All physicochemical and thermal property measurements above were performed at least three times, with deviations from the averages within ±3% for all extracted data.

Raman spectra were collected with a Bruker MultiRam FT-Raman spectrometer equipped with a liquid nitrogen cooled germanium detector, excited by the 1064 nm line of a Nd:YAG laser. A laser power of 400 mW, a spectral resolution of 2 cm^{-1}, and 500 scans were employed. The spectra were recorded in the range of 100–3600 cm^{-1}. Each sample was put in a glass vial with a screw lid under Ar atmosphere and transferred to the Raman set-up. The intensity of the Raman spectra for the ternary electrolytes was normalized with respect to the Raman band at 759 cm^{-1} (assigned to the

δCF_3 bending mode of the $[TfO]^-$ anion),[30] on the basis of salt concentration. For spectroscopic analysis, the normalized spectra were deconvoluted by Voigt functions with suitable Gaussian-Lorentzian ratios. Fourier-transform infrared (FT-IR) spectroscopy was carried out using a Bruker ALPHA spectrometer and a diamond ATR crystal. A spectral resolution of 4 cm^{-1} and 200 scans were employed. The FT-IR spectra were normalized on the basis of the peak observed at 1411 cm^{-1}, attributed to the NCH_3 symmetric band of NMA[31] and x_{NMA}. To avoid contamination, all measurements were conducted inside the Ar-filled glovebox. All spectroscopic measurements were performed at ambient temperature.

Electrochemical characterization was performed on the optimized ternary electrolyte and the EMIm/$AlCl_3$ acidic mixture using a three-electrode cell with a Gamry Reference 600 potentiostat/galvanostat/ZRA. A Pt disk (1.58 mm radius) working electrode, Al coil and Pt wire counter electrodes, and an Al wire reference electrode were used. The working electrode was polished with 1.0, 0.3, and 0.05 μm alumina paste prior to any experiments. The Al electrodes were soaked in a mixture of H_2SO_4/H_3PO_4/HNO_3 (25/70/5 by volume) for 15 minutes to remove the residual oxide, then washed with deionized water and dried under high vacuum immediately before the measurements. The electrochemical stability windows (ESWs) were evaluated by linear sweep voltammetry (LSV) with a scan rate of 10 mV s^{-1}. The limiting anodic and cathodic potentials were defined as the potentials where current densities of ±0.1 mA cm^{-2} were observed. Cyclic voltammetries (CVs) were measured at a scan rate of 20 mV s^{-1}. All electrochemical experiments were carried out inside the Ar-filled glovebox at ambient temperature.

Results and Discussions

1. Conventional non-aqueous organic electrolytes

Prior to treating the room temperature ternary electrolytes, it is useful to review physicochemical properties of conventional organic electrolytes containing $Al[TfO]_3$, as reference systems. In **Table 1**, we summarize the density (ρ), concentration (c), viscosity (η), ionic conductivity (σ), and molar conductivity (Λ) of such electrolytes with the same salt fraction ($x_{Al[TfO]3}$ = 0.05) including also a representative ternary electrolyte, **M**(0.760). In addition also the dielectric constants (ε_r) of the pure solvents used are tabulated. For the ternary electrolyte, a simple estimate model on the basis of individual ε_r values and the relative fraction of individual components was used.[32]

Table 1 Physicochemical properties of different $Al[TfO]_3$-containing electrolytes ($x_{Al[TfO]3}$ = 0.05) at 30 ºC.

Electrolyte*	ρ / g cm^{-3}	c / mol dm^{-3}	η / mPa s	σ / mS cm^{-1}	Λ / S cm^2 mol^{-1}	ε_r solvent @ 25 ºC
G1	1.00	0.456	0.855	0.52	1.1	7.07[33]
G3	1.05	0.271	2.99	0.12	0.45	7.63[33]
G4	1.06	0.226	4.63	0.041	0.18	7.78[34]
ACN	1.02	0.815	1.39	0.16	0.20	35.9[33]
PC	1.30	0.540	8.63	1.9	3.5	62.9[33]
NMA	1.11	0.597	33.4	2.4	4.0	178[35]
M(0.760)	1.16	0.638	53.8	2.5	3.9	81.3

* For DEC and THF as solvents no homogeneous electrolytes could be obtained, why these systems are excluded.

The electrolytes can roughly be divided into two groups on the basis of their conductivities; G1, G3, G4, and ACN vs. PC, NMA, and **M**(0.760). The former exhibit relatively low conductivities, less than 0.6 mS cm^{-1}, while the latter shows appreciable conductivities, above 1.5 mS cm^{-1}, at 30 ºC. Interestingly, the ternary electrolyte **M**(0.760) possesses the highest conductivity despite having the highest viscosity and hence lowest fluidity. For conventional electrolytes, it is well-known that conductivity is proportional/coupled to the fluidity. It should be noted that a binary mixture of the solvents NMA and urea with the same molar ratio as in **M**(0.760) exhibited negligible conductivity (*ca.* 10^{-6} mS cm^{-1}) even at 60 ºC, hence proving the high conductivity for **M**(0.760) to arise from the presence of $Al[TfO]_3$. The high conductivity for the NMA-based and ternary electrolytes could also suggest a minor contribution of proton conduction to the ionic conductivities, as the strong electric field of small and trivalent Al^{3+} ions could affect polarization of the solvated molecules, consequently leading to release free proton by solvolysis. Although the proton conduction coincides with the irregularly high conductivity, NMA and urea are not likely to react with $Al[TfO]_3$ during the sample preparation as organic compounds including acylamino-based are stable even towards $AlCl_3$,[16–18,27] known as a strong Lewis acid. In addition, the relatively large pK_a of conventional acylamino-based compounds, around 25 in dimethylsulfoxide,[36,37] indicates a poor proton donating ability and hence a low ability to generate protonated solvents. Taken altogether this strongly suggests a different (degree of) dissociation of $Al[TfO]_3$ and/or a different ionic conduction mechanism between the two groups and especially for the **M**(0.760) electrolyte.

The competition between ion–ion interactions and ion–solvent interactions determines the degree of salt dissociation. The Gutmann's donor number (*DN)* is a useful parameter in order to understand the relative solvating power (or simply Lewis basicity) of solvents. The *DN*s for G1, G3, G4, ACN, and PC are 18.6, 14.0, 16.6, 20.5, and 15.7, respectively.[38] Unfortunately, the *DN*s of NMA and urea have not been reported, but their analogues are known to have *DN*s of *ca.* 28–29, almost irrespective of substituents.[39] While we do not find the *DN*s to directly correlate to high conductivities (**Table 1**), a better trend was clearly observed using the dielectric constant (ε_r) of the solvents. Solvents with high dielectric constants can relax the strong electric field induced by charged species, thereby weakening the ion-ion interactions and consequently dissociate salts into their constituent ions. Thus, and as found in **Table 1**, the electrolytes made from solvents of relatively low ε_r possess lower conductivities, likely due to poor dissociation of Al[TfO]$_3$. The unexpectedly high conductivity for the G1-based electrolyte compared to *e.g.* ACN-based can be explained in terms of a chelating effect; bidentately coordinating G1 solvent molecules can solvate Al^{3+} ions more effectively than monodentately coordinating ACN. The relatively lower conductivity for G3 and G4 based electrolytes are attributable to a competition among concentration, viscosity, and chelating effects. On the other hand, the electrolytes based on high ε_r solvents show high conductivities; for example PC is a standard polar solvent for various electrolytes and readily dissociate even multivalent salts. NMA also functions as a solvent for Al[TfO]$_3$ as well as for Li salts.[24] Partial substitution of NMA by urea facilitates dissociation of Al[TfO]$_3$, unexpectedly as the simple model ε_r value of the NMA/urea mixture (81.3) is considerably lower than that of pure NMA

(178) (**Table 1**). This strongly suggests that urea affects the dielectric properties of NMA in a non-trivial manner, as also previously reported for urea in water to enhance the dielectric properties of water,[40,41] while the exact role of urea in the water/urea mixtures still is controversial.[42–44] Owing to the "water-like" physicochemical properties of NMA, a similar phenomenon may thus possibly occur in NMA/urea mixtures and result in appreciably higher dissociation of $Al[TfO]_3$ in the ternary electrolyte.

To further evaluate the state of $Al[TfO]_3$ in the different electrolytes a Walden plot was made (**Fig. 1**). For the ternary electrolyte systems, the variation of data arises both from changing composition and temperature. In general, an ideal KCl aqueous solution provides an ideal straight line with a slope of unity in Walden plots, and the dissociativity of other salts is evaluated based on the deviation from this ideal line. In the case of trivalent salts, however, such an ideal line is not relevant, and thus excluded from the figure, but still data located in the upper-left part of the plot indicates ion-ion dissociation and lower-right formation of neutral species *i.e.* association.

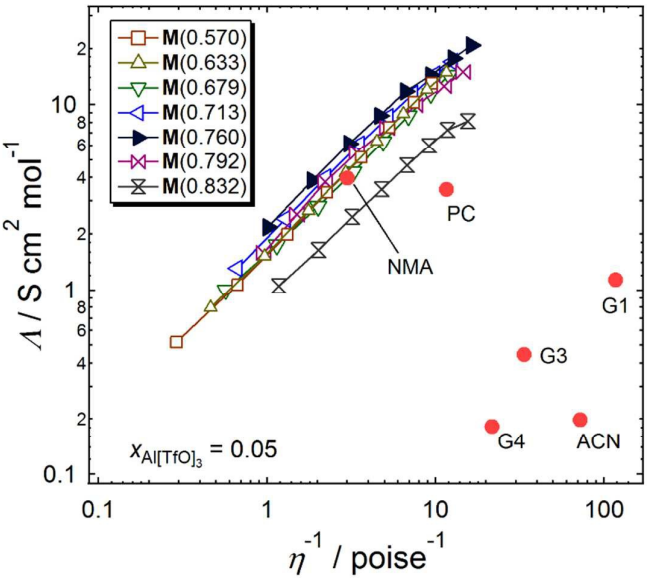

Fig. 1 Walden plot of the $Al[TfO]_3$-containing conventional electrolytes and ternary electrolytes.

From **Fig. 1** it is clear that the electrolytes can be divided into two groups, consistent with the sub-division on the basis of σ (*vide supra*). $Al[TfO]_3$ is most associated in ACN and substantial dissociation is observed for the most promising electrolytes. Although the NMA based electrolyte show higher Λ than **M**(0.760) (**Table 1**), the Walden plot strongly implies large dielectric properties of the NMA/urea mixtures. A remarkable finding for the ternary electrolytes is the strong relation between composition and dissociation; a subtle substitution of NMA by urea (**M**(0.832)) reduces the dissociation in comparison with pure NMA, while further substitution improves the dissociation, surpasses pure NMA, and reaches a maximum for **M**(0.760). Even more urea substitution, however, results in worse dissociation. The origins and practical implications of this complicated phenomenon will be treated in detail in the following section as it is the very basis for the use of ternary electrolytes as Al conductive electrolytes.

2. Room temperature ternary electrolytes

As described above, partial substitution of NMA by urea improves the dissociation of $Al[TfO]_3$. To further clarify the correlation between dissociation of $Al[TfO]_3$ and the composition of ternary electrolytes, a series of ternary electrolytes was prepared and characterized with respect to physicochemical properties and by vibrational spectroscopy.

Fig. 2a shows the variation of σ and η for the ternary electrolytes in the x_{NMA} range of 0.475–0.832 and at 30 ºC. The corresponding temperature dependent Arrhenius plots of η and σ are depicted in **Fig. 2b** and **2c**, respectively. All electrolytes show appreciably high σ, irrespective of composition. Preceding work on room-temperature binary systems incorporating urea or NMA revealed that the polar groups (C=O and NH) in these acylamino compounds are capable of coordinating cations and anions, and these interactions would relax both hydrogen-bonding interactions between organic compounds and ion-ion interactions leading to salt dissociation.[22,24] Here a composition dependence was observed for the ternary electrolytes; η gradually increases by the urea fraction, except for the system at x_{NMA} = 0.76 (**M**(0.760)) for which a small "kink" is observed (**Fig. 2a**). The composition dependence is, however, much more drastic for σ. A minute substitution of NMA by urea (**M**(0.832)) decreased σ as compared to the urea-free electrolyte (NMA, 2.381 mS cm^{-1} at 30 ºC), but in general the σ of the ternary electrolytes increased with the amount of urea ($0.118 < x_{urea} \leq 0.19$) until a clear and distinct maximum is observed at x_{NMA} = 0.76 (x_{urea} = 0.19). Further addition of urea, however, results in a decreased conductivity. This further supports the findings of the Walden plot (**Fig. 1**) and the optimal composition being **M**(0.760).

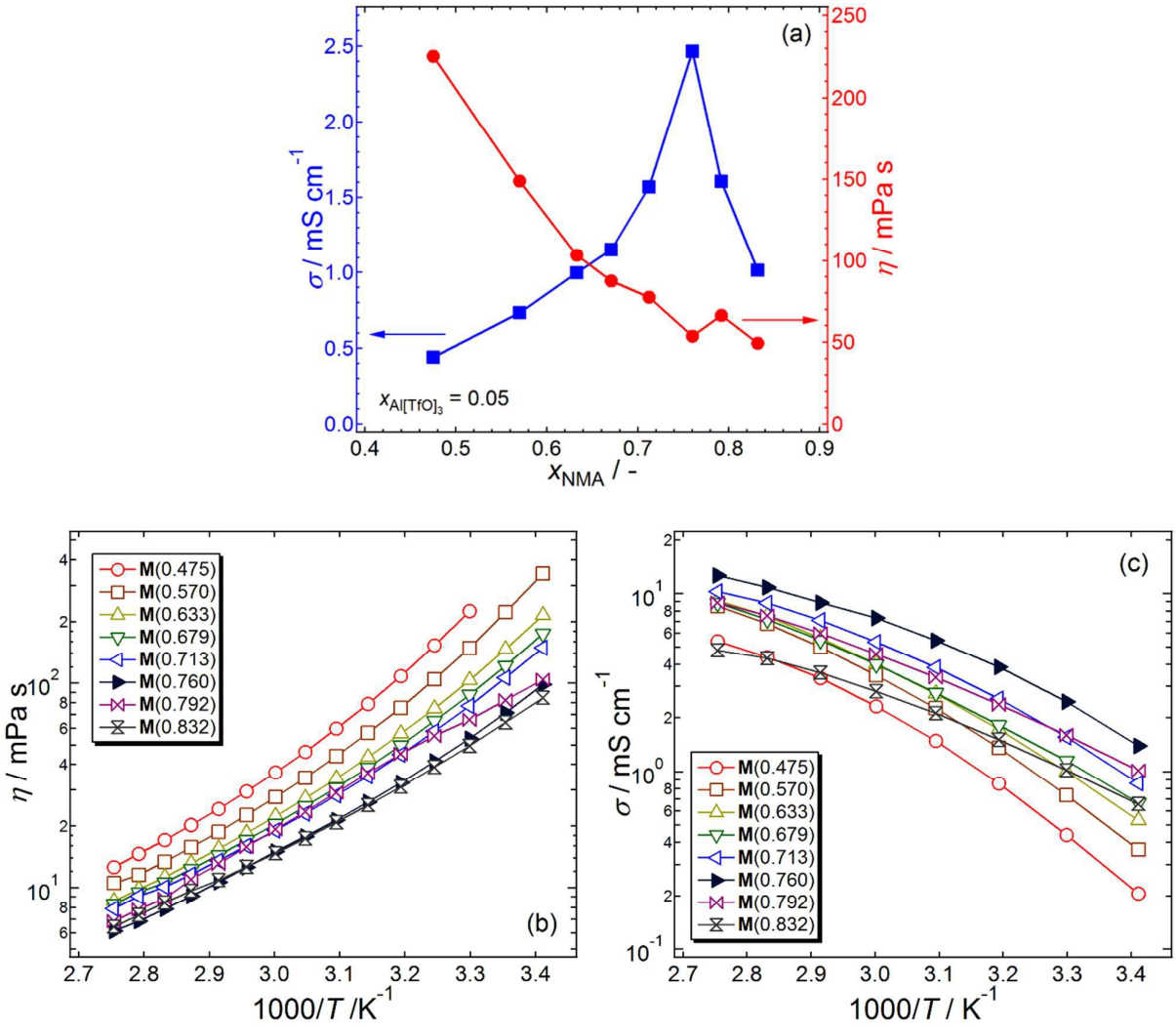

Fig.2 (a) Variation of ionic conductivity (σ) and viscosity (η) for the ternary electrolytes as a function of x_{NMA} at 30 ºC; Arrhenius plots of (b) η and (c) σ in the range 20–90 ºC.

Unlike the structurally analogous Mg-based ternary systems,[26] we find the temperature dependence of both η and σ to show non-Arrhenius, concave- and convex-curved, respectively, profiles as described by the following Vogel-Tammann-Fulcher (VTF) equations:

$$\eta = \frac{\sqrt{T}}{A_\eta} \exp\left[\frac{B_\eta}{T - T_{0,\eta}}\right]$$

$$\sigma = \frac{A_\sigma}{\sqrt{T}} \exp\left[\frac{-B_\sigma}{T - T_{0,\sigma}}\right]$$

where A_η and A_σ are scaling factors, B_η and B_σ are constants related to the activation energy for the

appropriate transport properties, and $T_{0,\eta}$ and $T_{0,\sigma}$ are the ideal glass transition temperatures where translational motion and ionic conduction, respectively, are frozen. The best fit parameters of these VTF equations are tabulated in **Table 2**. Excellent correlations were found between the electrolyte composition and these parameters. The B_η gradually increase with increasing NMA fraction in the electrolytes, while $T_{0,\eta}$ reaches a minimum plateau for **M**(0.760). In stark contrast, $T_{0,\sigma}$ does not reach any such plateau. The difference between $T_{0,\eta}$ and $T_{0,\sigma}$ expressed as $|T_{0,\sigma}-T_{0,\eta}|$ as a function of x_{NMA} is therefore provided in **Fig. 3**. The composition dependent glass transition temperatures (T_g) are also included in the figure. The DSC traces are provided in **Fig. S1**. As $T_{0,\sigma}$ and $T_{0,\eta}$ are indicative of the ideal temperatures where the corresponding processes are completely frozen, $|T_{0,\sigma}-T_{0,\eta}|$ can be regarded as an indicator to estimate how the ionic conduction process is dominated by translational dynamics of mobile species in the electrolytes. A relatively small deviation of the $|T_{0,\sigma}-T_{0,\eta}|$ value from zero, as observed for the systems containing large amounts of urea ($x_{\mathrm{NMA}} \leq 0.713$), means that ionic conduction in these electrolytes arises almost directly from translational dynamics. Similar deviations have been observed for ionic liquids and related condensed ionic materials.[45–49] In contrast, an exceptionally large $|T_{0,\sigma}-T_{0,\eta}|$ is observed for **M**(0.760). This strongly suggests the ionic conduction to occur by a solvent-assisted charge transport mechanism for the **M**(0.760) system. Moreover, in **Fig. 3** the composition dependent variations for both $|T_{0,\sigma}-T_{0,\eta}|$ and T_g show similar features as those for σ and η (**Fig. 2a**), understandable as T_g is closely related to the fluidity[50] and hence an electrolyte composition, where the conduction mechanism (or translational dynamics) and fluidity drastically change, is likely present.

Table 2. VTF equation parameters from the fit of temperature-dependent η and σ data. R^2 denotes correlation coefficient.

M(x_{NMA})	ln A_η	B_η / K	$T_{0,\eta}$ / K	R^2	ln A_σ	B_σ / K	$T_{0,\sigma}$ / K	R^2
M(0.475)	9.34	638	216	0.999	1.42	525	219	0.993
M(0.570)	9.44	636	212	0.999	2.42	671	204	0.998
M(633)	9.85	726	200	0.999	2.29	656	200	0.999
M(0.679)	9.71	702	199	0.999	2.78	846	177	0.999
M(0.713)	7.73	708	196	0.999	1.20	404	219	0.998
M(0.760)	10.6	920	174	0.999	0.705	285	229	0.999
M(0.792)	10.4	916	175	0.989	1.98	684	180	0.999
M(0.832)	10.3	876	173	0.999	0.308	415	207	0.995

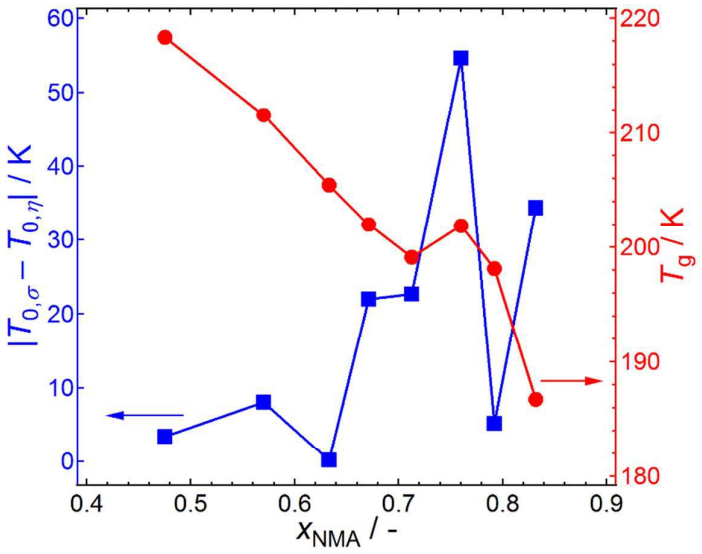

Fig. 3 Variation of $|T_{0,\sigma}-T_{0,\eta}|$ and T_g for the ternary electrolytes as a function of x_{NMA}

To elucidate how the composition affects the translational motion, the fluidity of the different ternary electrolytes was investigated in a T_g scaled Arrhenius plot (**Fig. 4**). In this manner different liquids can be compared on a common scale (T_g/T) and result in ionic liquids of high T_g to have

comparatively high fluidities.[50] Equivalently, the ternary electrolytes with high T_g are likely to possess high T_g-scaled fluidities, and again there is an exception for **M**(0.760), which has a high fluidity in spite of its relatively low T_g. This further supports its transport mechanism to be distinctly different compared to the other systems.

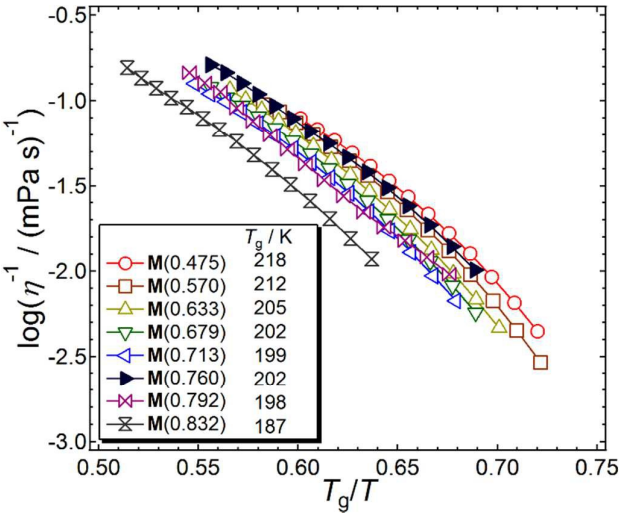

Fig. 4. T_g-scaled Arrhenius plots of fluidity for the ternary electrolytes with different compositions.

In general, macroscopic liquid properties are dependent on the microscopic liquid structure and interactions among constituents. As ionic conduction arises from the dynamics of ionic species, the salt dissociation state has a significant impact on the ionic conductivity. By vibrational spectroscopy, bands related to Al^{3+} coordination are used to study the variation of the coordination environment. Using FT-IR spectroscopy, the Al–O stretching mode, ν_s(Al–O), at around 650 cm^{-1},[51,52] is extremely difficult to use to distinguish between bands arising from Al–[TfO], Al–NMA, and Al–urea solvate species, as all may overlap. The complexation of NMA and urea with metal ions and the variation in hydrogen-bond strengths in the medium should affect the C=O and N–H stretching modes significantly.[53–55] Although the ternary electrolytes do provide distinct spectra from all individual

components and this indicates changes in the Al^{3+} coordination and deformation of the hydrogen-bonding network, all arising from altered interactions between solvents (NMA and urea), Al^{3+} cations, and $[TfO]^-$ anions, the precise assignment of composition dependent frequency shifts becomes ambiguous – as also these modes heavily overlap (**Fig. S2**).

In contrast, the Raman active symmetric SO_3 stretching mode, $\nu_s(SO_3)$, of the $[TfO]^-$ anions is particularly sensitive to coordination changes, and neither pure NMA or urea disturb the analysis of this mode. The $\nu_s(SO_3)$ mode for "free", or solvent-separated ion pairs (SSIPs), not coordinating to metal ions, $[TfO]^-$ anions is located at 1032 cm^{-1}; contact ion-pairs (CIPs) and higher aggregates for Li[TfO] are found at higher frequencies, 1041 and 1052 cm^{-1}, respectively.[56] Complexes with trivalent metal cations, such as Eu^{3+}, Nd^{3+}, and Ce^{3+} in poly (ethylene oxide), PEO, matrices provide complicated spectra, in which bands attributable to ion-ion-solvent complexes ($[M^{III}(TfO)_1]^{2+}$–PEO and/or $[M^{III}(TfO)_2]^{+}$–PEO) appear at around 1020 cm^{-1}, in addition to the bands for SSIPs (1032 cm^{-1}) and CIPs (1041 cm^{-1}).[56,57] When Li[TfO] is dissolved in different aprotic solvents SSIPs, CIPs, and aggregates provide bands at 1032, 1041, and 1050 cm^{-1}, respectively.[58] The dissociation state of the $Al[TfO]_3$ salt in the ternary electrolytes was elucidated primarily based on these preceding studies on $[TfO]^-$ band assignments.

The composition dependence of the $\nu_s(SO_3)$ modes in the Raman spectra is summarized in **Fig. 5**. The full band maximum is clearly observed at 1032 cm^{-1} irrespective of composition. With decreasing x_{NMA} (substituting NMA by urea), this band intensity gradually decreases, and simultaneously a broad shoulder located at the high-frequency side emerges, and hence the

dissociation state of $Al[TfO]_3$ in the ternary electrolytes is indeed composition dependent.

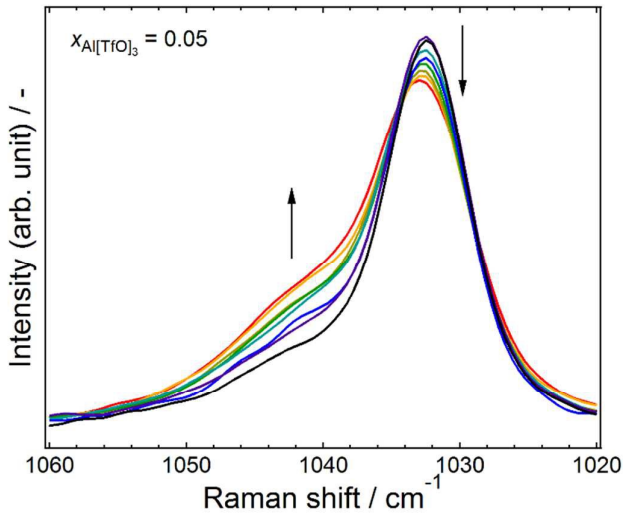

Fig.5 Composition dependence of Raman spectra in the range 1070–1010 cm^{-1} for the ternary electrolytes. The arrows indicate decreasing the NMA (increasing the urea) fraction in the systems.

A deconvolution and fitting of the spectra revealed the presence of two or three components (**Fig. 6**). Re-assuringly, the positions of the deconvoluted bands are insensitive to the electrolyte composition and number of bands needed for the fit. For a relatively small amount of urea (**Fig. 6a**, **M**(0.760)), the spectrum can be deconvoluted into three bands at 1032, 1041, and 1052 cm^{-1}, easily assignable to SSIPs, CIPs, and aggregates, respectively.[56,58] The relative intensities of the bands at 1052 cm^{-1} ($A_{1052\ cm-1}$ / $A_{total} \approx 2\%$) and 1041 cm^{-1} ($\approx 24\%$) suggest the $[TfO]^-$ anions to mainly exist as "free" anions/SSIPs. In the case of even larger amounts of urea, **M**(0.671), there are only two bands, at 1032 and 1041 cm^{-1}, in the deconvoluted spectrum (**Fig. 6b**). The variation of the relative intensities for each band (A_{band} / A_{total}) as a function of x_{NMA} is presented in **Fig. 6c**, and this clearly illustrates the presence of a composition where the dissociation state of $Al[TfO]_3$ drastically changes. This composition agrees well with that where various physicochemical properties drastically change

(*vide supra*). $Al[TfO]_3$ is highly dissociated in the systems with $x_{urea} \leq 0.19$ ($x_{NMA} \geq 0.76$). Further addition of urea facilitates association of $Al[TfO]_3$ although obviously small amounts of urea function to actually improve the dielectric properties of NMA (**Fig. 1**). Moreover, as stated before, NMA and urea are likely to possess similar *DN*s,[39] implying comparable capability for Al^{3+} solvation. In fact, both NMA and urea molecules are known to coordinate to various metal ions including Al^{3+} ion in a similar fashion, forming complexes.[55,59–63] Similar features were also observed for binary mixtures of LiTFSA/LiTFSI and glymes.[48,64] The dissociativity (termed "ionicity") maxima were in those studies found for critical compositions and explained in terms of multiple functions of the glyme solvents; glymes initially complex with Li^+ ions leading to salt dissociation, but further addition of these low dielectric glyme solvents (ε_r ~7) leads to salt association.[64] For our ternary system, the preferential coordination number for Al^{3+} is 4–6, and the molar ratio Al:NMA:urea in the **M**(0.760) electrolyte is 1:15:4. Although the precise coordination of Al^{3+} ions in the ternary electrolytes is ambiguous to determine due to overlapping of spectra (*vide infra*), the 1:4 ratio of Al:urea is perhaps no pure coincidence.

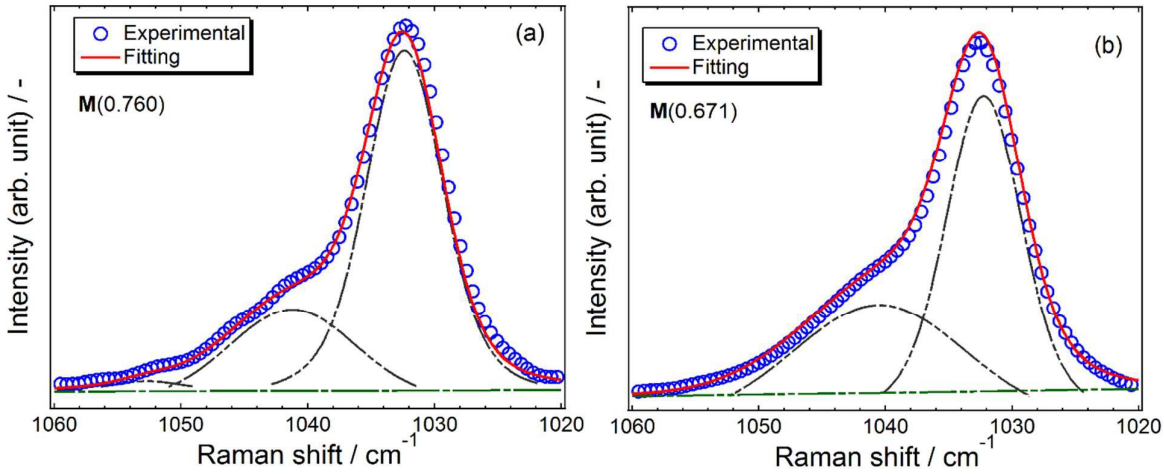

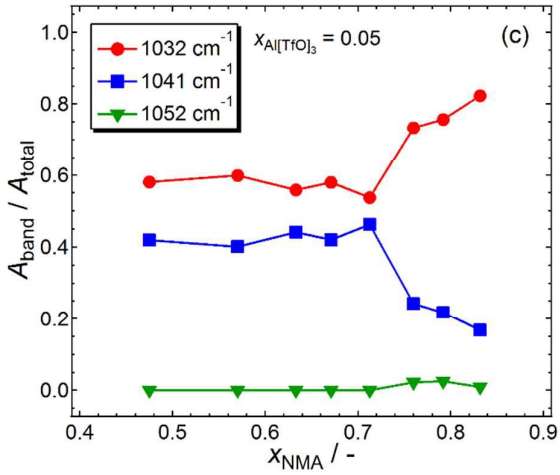

Fig. 6 Deconvolution results of Raman spectra into two or three components at around 1032, 1041, and 1052 cm^{-1} by Voigt functions for (a) x_{NMA} = 0.76 and (b) x_{NMA} = 0.671 ternary electrolytes. (c) Variations of the relative intensities of the 1032, 1041, and 1052 cm^{-1} bands as a function of x_{NMA} for the ternary electrolytes.

An electrochemical analysis was conducted to investigate the possibilities of the materials as Al battery electrolytes, and hence the optimized ternary electrolyte, **M**(0.760), was characterized with respect to the electrochemical stability windows (ESWs) and by cyclic voltammetry (CV), and subsequently compared with an EMImCl/$AlCl_3$ = 1/1.5 acidic melt, a commonly used and well-characterized electrolyte for Al batteries.[10,14,29,65,66]

The ESWs of the **M**(0.760) and the EMImCl/$AlCl_3$ reference electrolytes were obtained by linear sweep voltammetry (LSV). As shown in **Fig. 7**, the ESW of **M**(0.760) is obviously larger than that of EMImCl/$AlCl_3$; *ca.* 3.5 V for the former and *ca.* 2.3 V for the latter. The ESW of EMImCl/$AlCl_3$ agrees well with preceding work on imidazolium-based chloroaluminate ionic liquids.[14,65] The cathodic limiting potential for EMImCl/$AlCl_3$ is extremely narrow due to Al electroplating without polarization. On the other hand, for **M**(0.760), the anodic limiting potential, *ca.* 2.8 V vs. Al, is consistent with the values reported for urea containing electrolytes, suggesting

that the sharp rise in anodic current arises from an oxidative decomposition of urea (and/or NMA).[47] During the cathodic scan, the reductive current response at *ca.* −0.7 V probably results from Al electroplating, but electrochemical reduction of urea and NMA is likely to take place almost simultaneously, as small bubbles evolve on the Pt working electrode at *ca.* −1.2 V.

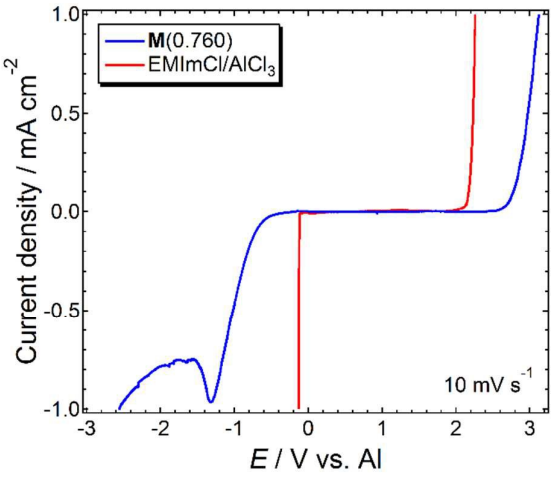

Fig. 7 LSV for the **M**(0.760) and the EMImCl/$AlCl_3$ reference electrolytes at ambient temperature. A Pt disk, a Pt wire, and an Al wire were employed as a working, counter, and quasi-reference electrodes, respectively.

The large ESW and relatively high ionic conductivity of **M**(0.760) offer the possibility of battery application. The electrochemical activity studied by CV is illustrated for the present and reference electrolyte in **Fig. 8a** and **8b**, respectively. While some reversible behavior can be observed for **M**(0.760) electrolyte, its response is considerably smaller than that for EMImCl/$AlCl_3$. The electrochemically active aluminum species in the acidic EMImCl/$AlCl_3$ melt are mainly $Al_2Cl_7^-$ ions, hence responsible for the reversible electroplating and stripping.[14,67,68] In stark contrast, the electrochemistry for the ternary electrolyte differ completely owing to absence of any chloroaluminate ions in the electrolyte. As described earlier, Al[TfO]$_3$ is well-dissociated and hence Al^{3+} ions exist as solvated ions especially in the optimized ternary electrolyte, **M**(0.760). In such

cases, Al electroplating at the electrolyte | electrode interfaces is considered to proceed through desolvation of solvents and subsequent Al^{3+} reduction. The reverse reactions may take place during the stripping process. As NMA and urea strongly coordinate to Al^{3+} ions in **M**(0.760), the desolvation process requires a large polarization, possibly resulting in a large overpotential. The rather poor current densities and cycling efficiency for **M**(0.760) can in part also be explained by side reactions, maybe a reductive decomposition of the electrolytes, taking place simultaneously with the plating during the cathodic scan.

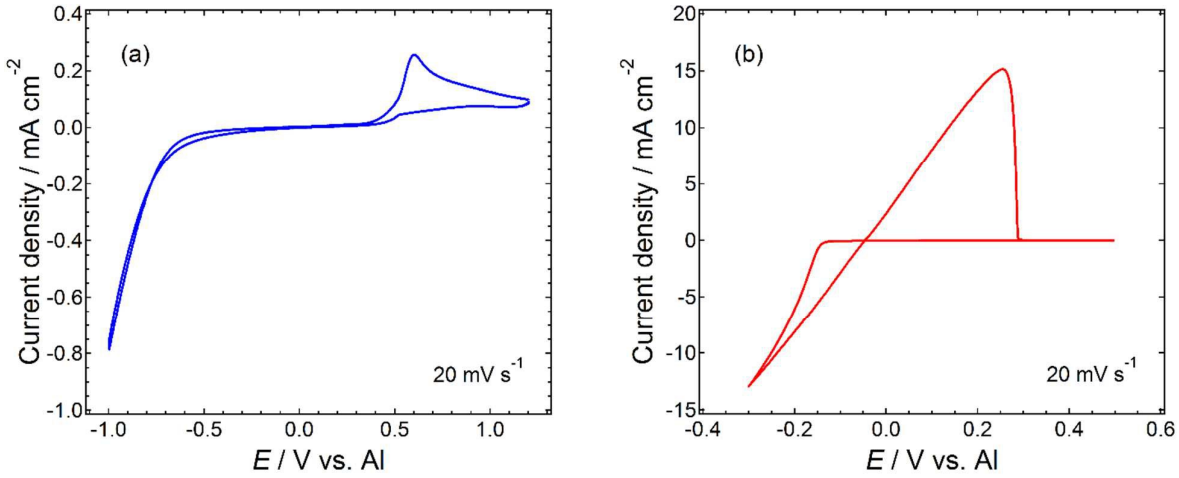

Fig. 8 Cyclic voltammograms recorded on a Pt electrode in (a) **M**(0.760) and (b) EMImCl/$AlCl_3$ acidic melt. Al wire was used as both counter and quasi-reference electrodes.

Summary

A series of room temperature ternary electrolytes composed of $Al[TfO]_3$, *N*-methylacetamide (NMA), and urea were characterized with respect to the physicochemical and electrochemical properties and by vibrational spectroscopy. Comparison of the various properties with those of organic electrolytes revealed excellent solvation ability of the NMA/urea mixtures for the trivalent

Al salt. The NMA/urea ratio has significant effect on the solvation ability. For the mixtures with low urea fraction ($x_{urea} \leq 0.19$), urea functions to improve the dielectric properties of NMA and facilitates dissociation of $Al[TfO]_3$, consequently increasing the ionic conductivity. As the urea fraction is further increased, however, the relatively low polar urea promotes salt association. The composition where the dissociation state of $Al[TfO]_3$ changes agrees well with that where various physicochemical properties drastically change; at an optimal composition of **M**(0.760). Moreover, VTF parameters and the fluidity of the **M**(0.760) electrolyte further support its ionic conduction to occur by a solvent-assisted charge transport mechanism, induced by substitution of NMA by urea. The preferential coordination of Al^{3+}, a favorable Al:urea ratio, and the multiple functions of urea all contribute to these composition dependent features for the ternary electrolytes. The electrochemical properties of the optimized ternary electrolyte **M**(0.760), characterized by LSV and CV measurements, were compared with the chloroaluminate-based ionic liquid electrolyte $EMImCl/AlCl_3$, to investigate its potential as an Al battery electrolyte. The LSV results indicated a substantially large ESW for **M**(0.760). Despite the large ESW and relatively high ionic conductivity, **M**(0.760) was modestly active electrochemically as compared to $EMImCl/AlCl_3$, possibly due to the strong solvation by NMA and urea solvent molecules of the Al^{3+} ions. The electrochemically reversible behavior observed in the **M**(0.760) electrolyte, however, opens new possibilities to create Al-conductive electrolytes independent of any extremely sensitive haloaluminate species. Furthermore, this study is the first demonstration of the versatility and excellent performance of especially tailored NMA/urea mixtures as solvents for multivalent salts.

Acknowledgement

The financial support by Chalmers Area of Advance Materials Science and the Swedish Energy Agency ("Batterifonden") is gratefully acknowledged. PJ is also thankful for the continuous support by Chalmers Area of Advance Energy and Transport.

Supporting Information

DSC traces of the ternary electrolytes with different compositions are provided in **Fig. S1**. FT-IR spectra in the range 1700–1500 cm^{-1} for the pure components (NMA, urea, and $Al[TfO]_3$) and for different ternary electrolytes are provided in **Fig. S2**.

References

1. J. Muldoon, C. B. Bucur, T. Gregory, *Chem. Rev*. 2014, **114**, 11683–11720.

2. P.-J. Alarco, Y. A.-Lebdeh, A. Abouimrane, M. Armand, *Nat. Mater*. 2004, **3**, 476–481.

3. S. H. Lapidus, N. N. Rajput, X. Qu, K. W. Chapman, K. A. Persson, P. J. Chupas, *Phys. Chem. Chem. Phys*. 2014, **16**, 21941–21945.

4. O. Bortolini, C. Chiappe, T. Ghilardi, A. Massi, C. S. Pomelli, *J. Phys. Chem. A*, doi: 10.1021/jp507437g.

5. D. Aurbach, Z. Lu, A. Schechter, Y. Gofer, H. Gizbar, R. Turgeman, Y. Cohen, M. Moshkovich, E. Levi, *Nature* 2000, **407**, 724–727.

6. Z. Z.-Karger, X. Zhao, O. Fuhr, M. Fichtner, *RSC Adv*. 2013, **3**, 16330–16335.

7. S.-Y. Ha, Y.-W. Lee, S. W. Woo, B. Koo, J.-S. Kim, J. Cho, K. T. Lee, N.-S. Choi, *ACS Appl. Mater. Interfaces* 2014, **6**, 4063–4073.

8. G. G. Kumar, N. Munichandraiah, *Electrochim. Acta* 2002, **47**, 1013–1022.

9. A. Guerfi, J. Trottier, I. Boyano, I. D. Meatza, J. A. Blazquez, S. Brewer, K. S. Ryder, A. Vijh, K. Zaghib, *J. Power Sources* 2014, **248**, 1099–1104.

10. N. Jayaprakarsh, S. K. Das, L. A. Archer, *Chem. Commun*. 2011, **47**, 12610–12612.

11. D. Linden, T. B. Reddy, *Ed*., *Handbook of Batteries 3rd Edition*; *McGraw-Hill*: New York, USA, 2003.

12. K. Xu, *Chem. Rev*. 2014, **114**, 11503–11618.

13. A. Ponrouch, D. Monti, A. Boschin, B. Steen, P. Johansson, M. R. Palacin, *J. Mater. Chem. A* 2015, **3**, 22–42.

14. J. S. Wilkes, J. A. Levisky, R. A. Wilson, C. L. Hussey, *Inorg. Chem*. 1982, **21**, 1263–1264.

15. Y. Zhao, T. J. VanderNoot, *Electrochim. Acta* 1997, **42**, 1639–1643.

16. L. Legrand, M. Heintz, A. Tranchant, R. Messina, *Electrochim. Acta* 1995, **40**, 1711–1716.

17. L. Legrand, A. Tranchant, R. Messina, *Electrochim. Acta* 1996, **41**, 2715–2720.

18. H. M. A. Abood, A. P. Abbott, A. D. Ballantyne, K. S. Ryder, *Chem. Commun*. 2011, **47**, 3523–3525.

19. M.-F. Shu, H.-Y. Hsu, C.-C. Yang, *Z. Naturforsch* 2003, **58a**, 451–456.

20. K. L. Fow, M. Ganapathi, I. Stassen, J. Fransaer, K. Binnemans, D. E. D. Vos, *Chem. Commun*. 2013, **49**, 8498–8500.

21. R. Nikolić, G. Ristić, *Sol. Energ. Mat. Sol. C.* 1992, **28**, 59–69.

22. H. Liang, H. Li, Z. Wang, F. Wu, L. Chen, X. Huang, *J. Phys. Chem. B* 2001, **105**, 9966–9969.

23. Y. Hu, H. Li, X. Huang, L. Chen, *Electrochem. Commun*. 2004, **6**, 28–32.

24. A. Boisset, J. Jacquemin, M. Anouti, *Electrochim. Acta* 2013, **102**, 120–126.

25. R. Chen, F. Wu, H. Liang, L. Li, B. Xu, *J. Electrochem. Soc*. 2005, **152**, A1979–A1984.

26. N. S. V. Narayanan, B. V. A. Raj, S. Sampath, *J. Power Sources* 2010, **195**, 4356–4364.

27. A. P. Abbott, R C. Harris, Y.-T. Hsieh, K. S. Ryder, I.-W. Sun, *Phys. Chem. Chem. Phys*. 2014, **16**, 14675–14681.

28. G. F. Reynolds, C. J. Dymek, Jr., *J. Power Sources* 1985, **15**, 109–118.

29. J. V. Rani, V. Kanakaiah, T. Dadmal, M. S. Rao, S. Bhavanarushi, *J. Electrochem. Soc*. 2013, **160**, A1781–A1784.

30. W. Huang, R. Frech, R. A. Wheeler, *J. Phys. Chem*. 1994, **98**, 100–110.

31. X. G. Chen, R. S. Stenner, S. A. Asher, N. G. Mirkin, S. Krimm, *J. Phys. Chem*. 1995, **99**, 3074–3083.

32. B. R. Pujari, B. Barik, B. Behera, *Phys. Chem. Liq*. 1998, **36**, 105–112.

33. J.-L. M. Abboud, R. Notario, *Pure Appl. Chem*. 1999, **71**, 645–718.

34. C. F. Riadigos, R. Igresias, M. A. Rivas, T. P. Igresias, *J. Chem. Thermodyn*. 2011, **43**, 275–283.

35. J. Swiergiel, J. Jadzyn, *J. Chem. Eng. Data* 2009, **54**, 2296–2300.

36. F. G. Bordwell, *Acc. Chem. Res*. 1988, **21**, 456–463.

37. F. G. Bordwell, J. A. Harrelson, Jr., T.-Y. Lynch, *J. Org. Chem*. 1990, **55**, 3337–3341.

38. D. Brouillette, G. Perron, J. E. Desnoyers, *J. Sol. Chem*. 1998, **27**, 151–182.

39. Y. Marcus, *Chem. Soc. Rev*. 1993, **22**, 409–416.

40. J. Wyman, Jr., *J. Am. Chem. Soc*. 1933, **55**, 4116–4121.

41. D. B. Wetlaufer, S. K. Malik, L. Stoller, R. L. Coffin, *J. Am. Chem. Soc*. 1964, **86**, 508–514.

42. A. W. Hakin, C. L. Beswick, M. M. Duke, *J. Chem. Soc., Faraday Trans*. 1996, **92**, 207–214.

43. R. Zhang, G.-S. Zhao, W.-J. Wu, Chin. *J. Chem. Phys*. 2009, **22**, 511–516.

44. J. K. Carr, L. E. Buchanan, J. R. Schmidt, M. T. Zanni, J. L. Skinner, *J. Phys. Chem. B* 2013, **117**, 13291–13300.

45. H. Tokuda, K. Hayamizu, K. Ishii, M. A. B. H. Susan, M. Watanabe, *J. Phys. Chem. B* 2004, **108**, 16593–16600.

46. H. Tokuda, K. Hayamizu, K. Ishii, M. A. B. H. Susan, M. Watanabe, *J. Phys. Chem. B* 2005, **109**, 6103–6110.

47. L. Timperman, F. Béguin, E. Frackowiak, M. Anouti, *J. Electrochem. Soc*. 2014, **161**, A228–A238.

48. K. Yoshida, M. Tsuchiya, N. Tachikawa, K. Dokko, M. Watanabe, *J. Phys, Chem. C* 2011, **115**, 18384–18394.

49. T. Tsuda, K. Kondo, M. Baba, S. Suwa, Y. Ikeda, T. Sakamoto, S. Seino, H. Yoshida, M. Ozaki, A. Imanishi, S. Kuwabata, *Electrochim. Acta* 2013, **100**, 285–292.

50. W. Xu, K. I. Cooper, C. A. Angell, *J. Phys. Chem. B* 2003, **107**, 6170–6178.

51. L. Andrews, T. R. Burkholder, J. T. Yustein, *J. Phys. Chem*. 1992, **96**, 10182–10189.

52. Y. Nakayama, Y. Senda, H. Kawasaki, N. Koshitani, S. Hosoi, Y. Kudo, H. Morita, M. Nagamine, *Phys. Chem. Chem. Phys*. 2015, **17**, 5758–5766.

53. C. N. R. Rao, H. S. Randhawa, N. V. R. Reddy, D. Chakravorty, *Spectrochim. Acta* 1975, **31A**, 1283–1291.

54. A. M. Barrios, S. J. Lippard, *Inorg. Chem*. 2001, **40**, 1250–1255.

55. K. Lewinski, L. Lebioda, *J. Am. Chem. Soc*. 1986, **108**, 3693–3696.

56. G. Petersen, A. Brodin, L. M. Torell, M. Smith, *Soild State Ionics* 1994, **72**, 165–171.

57. G. Petersen, L. M. Torell, S. Panero, B. Scrosati, C. J. Silva, M. Smith, *Solid State Ionics* 1993, **60**, 55–60.

58. J. M. Alia, H. G. M. Edwards, *Vib. Spectrosc*. 2000, **24**, 185–200.

59. R. Chakrabarti, K. Venkatesan, C. N. R. Rao, *Proc. R. Soc. Lond. A* 1981, **375**, 127–153.

60. L. Lebioda, K. Lewinski, *Acta Cryst*. 1980, **B36**, 693–695.

61. L. Lebioda, *Acta Cryst*. 1977, **B33**, 1583–1586.

62. J. H. M. Mooy, W. Krieger, D. Heijdenrijk, C. H. Stam, *Chem. Phys. Lett*. 1974, **29**, 179–182.

63. K. Sarder, M. Dan, B. Schwenzer, C. N. R. Rao, *J. Mater. Chem*. 2005, **15**, 2175–2177.

64. C. Zhang, K. Ueno, A. Yamazaki, K. Yoshida, H. Moon, T. Mandai, Y. Umebayashi, K. Dokko, M. Watanabe, *J. Phys. Chem. B* 2014, **118**, 5144–5153.

65. P. R. Gifford, J. B. Palmisano, *J. Electrochem. Soc*. 1987, **34**, 610–614.

66. W. Wang, B. Jiang, W. Xiong, H. Sun, Z. Lin, L. Hu, J. Tu, J. Hou, H. Zhu, S. Jiao, Scientific Reports, doi: 10.1038/srep03383.

67. P. K. Lai, M. S.-Kazacos, *Electrochim. Acta* 1987, **32**, 1443–1449.

68. P. K. Lai, M. S.-Kazacos, *J. Electroanal. Chem*. 1988, **248**, 431–440.

Graphical Abstract

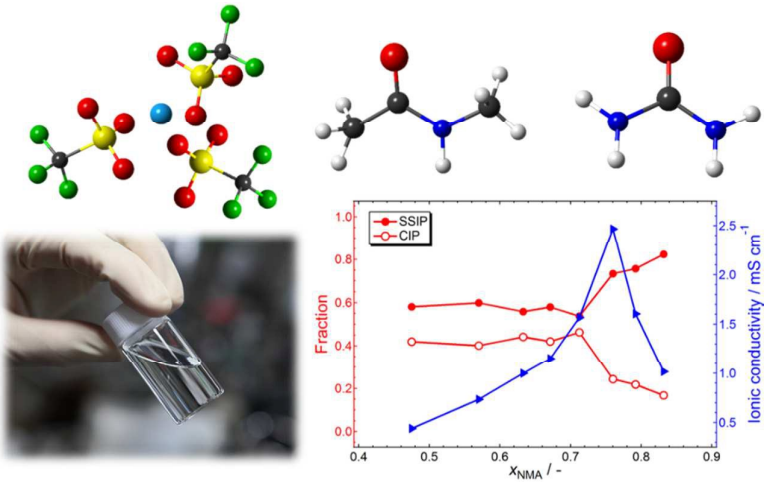

Appropriate combinations of aluminum trifluoromethanesulfonate, *N*-methylacetamide, and urea result in room temperature ternary electrolytes with high ionic conductivities.